

Halide Perovskites

International Edition: DOI: 10.1002/anie.201601788
German Edition: DOI: 10.1002/ange.201601788

Pressure-Dependent Polymorphism and Band-Gap Tuning of Methylammonium Lead Iodide Perovskite

Shaojie Jiang, Yanan Fang, Ruipeng Li, Hai Xiao, Jason Crowley, Chenyu Wang, Timothy J. White, William A. Goddard III,* Zhongwu Wang, Tom Baikie,* and Jiye Fang*

Abstract: We report the pressure-induced crystallographic transitions and optical behavior of MAPbI₃ (MA = methylammonium) using *in situ* synchrotron X-ray diffraction and laser-excited photoluminescence spectroscopy, supported by density functional theory (DFT) calculations using the hybrid functional B3PW91 with spin-orbit coupling. The tetragonal polymorph determined at ambient pressure transforms to a ReO₃-type cubic phase at 0.3 GPa. Upon continuous compression to 2.7 GPa this cubic polymorph converts into a putative orthorhombic structure. Beyond 4.7 GPa it separates into crystalline and amorphous fractions. During decompression, this phase-mixed material undergoes distinct restoration pathways depending on the peak pressure. *In situ* pressure photoluminescence investigation suggests a reduction in band gap with increasing pressure up to ≈0.3 GPa and then an increase in band gap up to a pressure of 2.7 GPa, in excellent agreement with our DFT calculation prediction.

Organic–inorganic metal halide perovskite-based photovoltaic (PV) cells show potential for the direct conversion of sunlight into electricity, as a result of their high charge-carrier

mobilities and electron/hole diffusion lengths of hundreds of nanometers.^[1–3] The power conversion efficiency (PCE) of perovskite PV cells has rapidly increased from about 6% in 2011 towards approximately 20% presently, although device reproducibility is questionable.^[3–8] The PCE can be enhanced by modifying charge-carrier mobility and the direct band gap through tuning crystal chemistry.^[9,10] Nonetheless, to date, extensive synthesis campaigns have revealed a limited range of materials. Alternatively, pressurization is a straightforward and robust way to transform crystal structures, where changes in bond strength and geometry are induced without the complication of chemical adjustments. By monitoring changes in photovoltaic properties, strategies for selecting ions of appropriate size and charge can be devised.^[11,12] To this end, pressure-dependent structural behaviors of stable and metastable polymorphs can guide design strategies.^[13]

The perovskite prototype has the general formula of ABX₃, where corner-sharing BX₆ octahedra create a 3D framework with an A component providing charge compensation if necessary (Figure 1a). The aristotype is cubic *Pm* $\bar{3}$ *m* (space group, No. 221), in which all the BX₆ octahedra show B–X–B angles of 90°. This arrangement of untitled octahedra can be described in Glazer notation^[14,15] as *a*⁰*a*⁰*a*⁰. Among the Pb-based methylammonium (MA) halide perovskites (ionic A = CH₃NH₃⁺ or MA; X = Cl[−], Br[−], I[−]; B = Pb²⁺), the band gaps of MAPbCl₃, MAPbBr₃, and MAPbI₃ are reported as around 3.1, 2.3, and 1.5 eV, respectively.^[10,16] For single junction PV cells a band gap in the range between 1.1 and

[*] S. Jiang, Prof. J. Fang

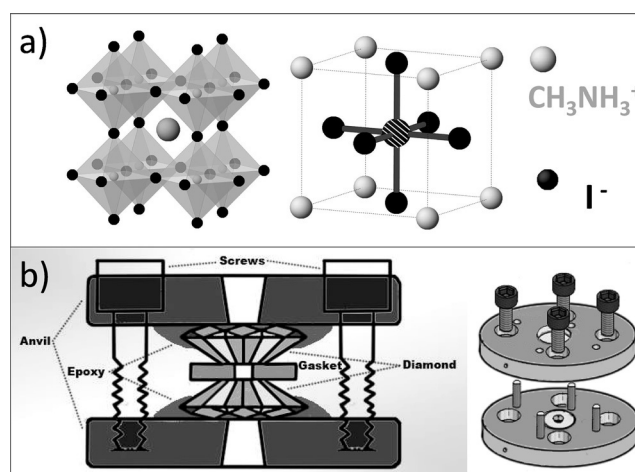
Materials Science and Engineering Program
State University of New York at Binghamton
Binghamton, NY 13902 (USA)
E-mail: jfang@binghamton.eduDr. Y. Fang, Dr. T. Baikie
Energy Research Institute@NTU (ERI@N)
Nanyang Technological University
50 Nanyang Drive, Singapore 637553 (Republic of Singapore)
E-mail: tbaikie@ntu.edu.sgDr. R. Li, Dr. Z. Wang
Cornell High Energy Synchrotron Source, Cornell University
Ithaca, NY 14853 (USA)Dr. H. Xiao, J. Crowley, Prof. W. A. Goddard III
Materials and Process Simulation Center (MSC) and Joint Center for
Artificial Photosynthesis (JCAP)
California Institute of Technology
Pasadena, CA 91125 (USA)
E-mail: wag@wag.caltech.eduDr. C. Wang, Prof. J. Fang
Department of Chemistry, State University of New York at Binghamton
Binghamton, NY 13902 (USA)Prof. T. J. White
School of Materials Science and Engineering, Nanyang Technological
University
Nanyang Avenue, Singapore 639798 (Republic of Singapore)Supporting information for this article can be found under:
<http://dx.doi.org/10.1002/anie.201601788>.

Figure 1. a) MAPbI₃ perovskite *Pm* $\bar{3}$ *m* polymorph (left, polyhedral model; right, with Pb–I bonds emphasized); b) Diamond anvil cells holder system with balanced compression screws (left: side view; right: top-down view).

1.4 eV is desired.^[17] Therefore, MAPbI₃ is the preferred material. Previous studies of pressure-induced transformations in hybrid perovskites illustrate the crystallographic richness and band-gap changes. Although pressure-induced synchrotron powder X-ray diffraction (XRD) of MAPbI₃ was reported recently,^[18] extraction of high-pressure lattice parameters, the unambiguous determination of crystal symmetry and the refinement of atomic fractional coordinate are challenging.

Herein we synthesize MAPbI₃ as reported previously.^[19] In brief, polycrystalline MAPbI₃ was precipitated by 6 h cooling from 100 to 46 °C after mixing PbI₂ and MA-I solutions in a Pyrex test tube. The PbI₂ solution was prepared by dissolving 2.5 g of lead(II) acetate (Chemical Reagents, Sigma–Aldrich)

in 10 mL of aqueous HI solution (57 wt %), whereas the MA-I solution was formed by dissolving 0.597 g of aqueous CH₃NH₂ solution (40 %, Merck) in 2 mL of HI solution. The diamond anvil cells (DACs) with a size of 500 μm were aligned, assembled, and pressurized before conducting XRD (Figure 1 b). A stainless-steel gasket was indented before drilling a roughly 200 μm diameter hole that served as the compaction chamber. Ruby fluorescence was used to calibrate pressure^[20] and ruby chips were distributed on the sample surface before closing the DAC. At each pressure, an XRD pattern ($\lambda = 0.485946 \text{ \AA}$) was collected at the B1 station of the Cornell High Energy Synchrotron Source (CHESS),^[21] with a data accumulation time of 10 mins at each pressure, after maintaining the pressure for approximate 20 min.

Synchrotron XRD patterns of MAPbI₃ collected at room temperature (Figure 2a) and ambient pressure confirms a tetragonal polymorph (*I4/mcm*, No. 140) with lattice constants of $a_t = 8.8648(6) \text{ \AA}$ and $c_t = 12.6746(8) \text{ \AA}$. For this phase, octahedral tilting is about the unique *c* axis only and the Glazer notation is $a^0a^0c^-$. For the tetragonal (*t*) heterotype derived from the cubic (*c*) aristotype, $a_t = a_c\sqrt{2}$ and $c_t = 2a_c$. At approximately 0.3 GPa, additional reflections appear at $2\theta \approx 7.1^\circ$ and 8.4° , which Pawley fitting (Figure S1 in the Supporting Information) shows to be consistent with a cubic bilayer supercell (*s*) (*Im* $\bar{3}$, No. 204), where $a_s = 2a_c$ as previously observed for the MAPbBr₃ analogue,^[22] and a high pressure polymorph of ReO₃, where A site in ABX₃

is vacant.^[23,24] No evidence was found for the *Pm* $\bar{3}m$ aristotype identified in a previous variable-temperature study.^[19] Although the *Pm* $\bar{3}m$ reflections may substantially overlap with those of the *Im* $\bar{3}$ supercell, the conventional primitive unit cell was not observed as a separate phase (Figure S1). For comparison, temperature-dependent XRD measurements were collected to 60 °C (Figure S2) to demonstrate reflections of the conventional *Pm* $\bar{3}m$ polymorph persist at elevated temperature (Figure 2a and Figure S2).

Beyond 0.4 GPa, MAPbI₃ completely transforms to the *Im* $\bar{3}$ phase with $a_s = 12.4076(8) \text{ \AA}$ and tilt character $a^+a^+a^+$, with octahedral tilt of equal magnitude about all three axes (Figure S1). For this polymorph, the cell volume contracts and the Bragg reflections broaden as a function of the applied pressure until 2.3 GPa. Prior to amorphization at 4.7 GPa, an additional phase appearing at 2.7 GPa was identified, with 00 l reflections becoming triply degenerate (Figure S3). Such splitting would be consistent with orthorhombic symmetry, and by analogy with MASnI₃^[25] may be an *Immm* (No. 71) polymorph with $a^+b^+c^+$ PbI₆ tilting. Reports of an orthorhombic high-pressure form of MAPbBr₃ remain ambiguous.^[22,26] Beyond 2.7 GPa MAPbI₃ continues to amorphize to near completion at 4.7 GPa, with no further change in X-ray scattering character up to 6.4 GPa (also refer to 2D diffraction patterns in Figure 2c). Upon a gradual release of pressure, the sample remains partially amorphous until 0.58 GPa without the appearance of the putative *Immm*

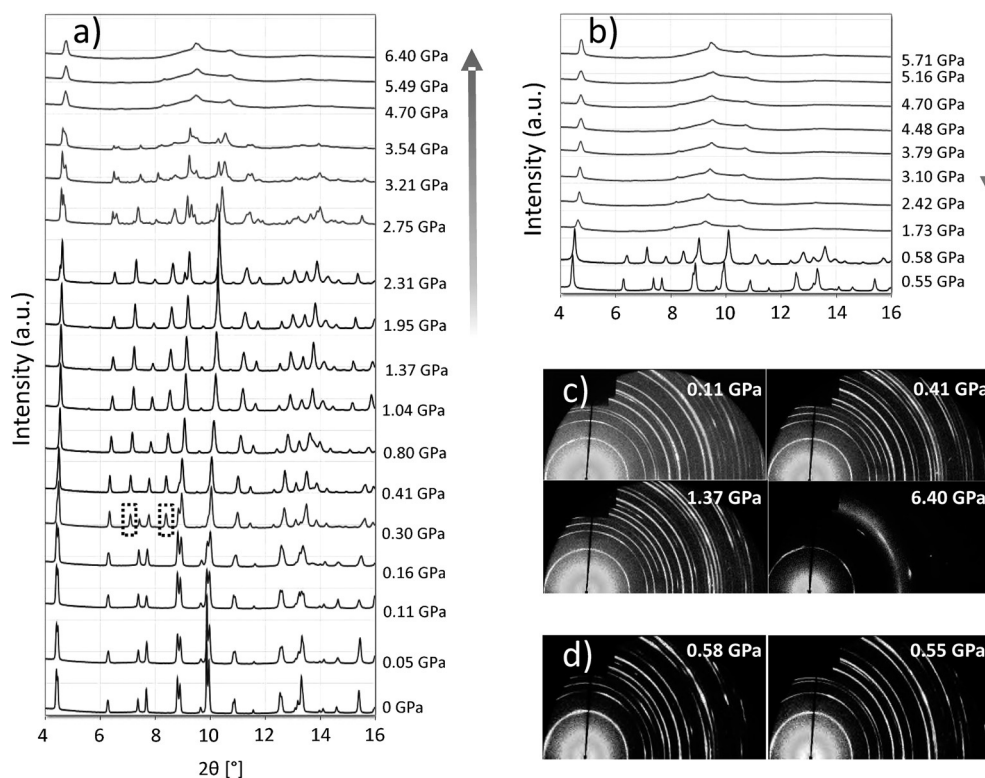


Figure 2. Conventional XRD patterns of MAPbI₃ during a) compression and b) decompression. a) The ReO₃-type cubic supercell (*a_s*) appears at 0.3 GPa (highlighted by broken-lined boxes) and becomes more abundant to 2.3 GPa, before conversion into the putative orthorhombic polymorph at 2.7 GPa, and finally approaches X-ray amorphicity above 3.5 GPa. b) Decompression from the amorphous mass restores the tetragonal phase at 0.58 GPa. c) and d) Representative 2D XRD patterns at specific pressures.

polymorph (Figure 2b). However, the $Im\bar{3}$ phase appeared at 0.58 GPa, and the $I4/mcm$ was restored at 0.55 GPa (Figure 2b,d).

To determine the influence of the maximum applied pressure and microstructural evolution during decompression, a series of experiments with different peak-pressures were conducted. For example, using 3.5 GPa as the peak pressure (Figure S4) the $Immm$ structure was favored at 2.8 GPa, and the $Im\bar{3}$ polymorph was recovered when the pressure was reduced to 0.9 GPa. This confirms the recovered structure during decompression is controlled by the peak pressure. The decompression pattern collected at 1.37 GPa was modelled using both $Immm$ and $Im\bar{3}$ polymorphs (Figure S5). However, the poor Pawley fit of the 004 reflection (at $2\theta \approx 9^\circ$) for the cubic polymorph indicates this phase(s) resides on the borderline of the orthorhombic–cubic transition. This evidence supports the existence of the $Immm$ polymorph, but suggests it is metastable with respect to the $Im\bar{3}$ and $I4/mcm$ polymorphs. The tetragonal structure forms reversibly when the applied pressure does not exceed 8.0 GPa. Taken alone, Pawley fitted cell metrics do not show a clear discontinuity as the symmetry varies (Figure S6), but optical microscopy does show some distinct changes (Figure S7).

Using the refined atomic fractional coordinates for Pb and I in the ReO_3 -type $Im\bar{3}$ cubic supercell as a basis, the octahedral topologies in the cubic (c), tetragonal (t), and ReO_3 -type cubic supercell (s) of the $MAPbI_3$ can be derived (Figure 3).^[24] It should be noted that only the MA groups are dynamic^[27] and not included. The octahedral tilt angle in the cubic supercells approaches around 15° in advance of the appearance of the orthorhombic polymorph (refer to Table S1).^[24] The CIFs generated from the density functional theory (DFT) calculations (see below) also show all the relevant coordinates (Table S2).

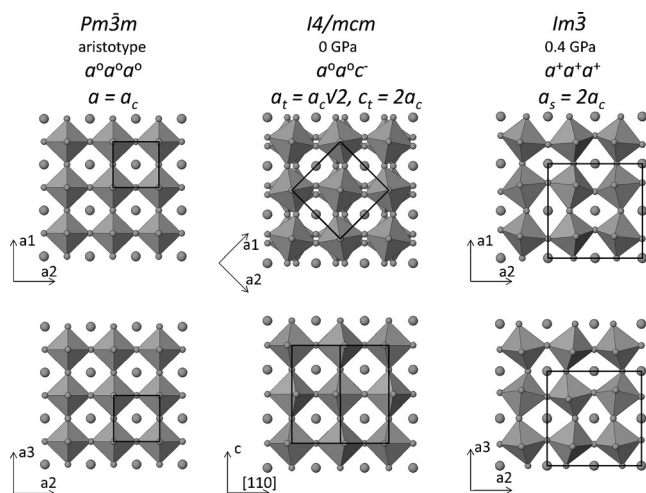


Figure 3. Characteristic PbI_6 octahedral and Glazer symbols of some typical pressure-related polymorphs. The image for $Immm$ polymorph should be similar to that of $Im\bar{3}$ with slightly different lattice parameters along each axis and an octahedral tilt change (Glazer symbol: $a^+b^+c^+$).

The $MAPbI_3$ polymorphs show discrete band gaps that can be calculated from in situ pressure-photoluminescence (PL) spectra during a compression (Figure 4a and Table S3)

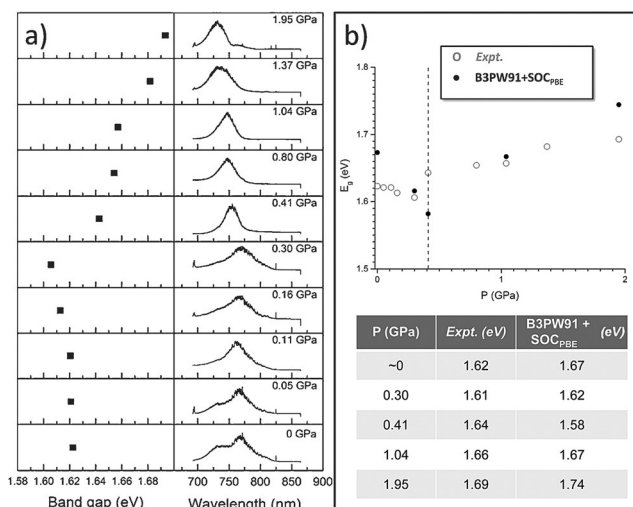


Figure 4. a) Measured photoluminescence spectra (right panel) and calculated band gaps (left panel) of $MAPbI_3$ as a function of compression pressure at room temperature. b) The band gaps determined by measurement and B3PW91 + SOC_{pBE} calculations (also refer to Table S2 in supporting information).

but are typically larger than those determined by absorption,^[28] as the Tauc plot^[29] was not calculated. At ambient conditions, the PL spectrum shows a broad band at 764 nm, equivalent to the band gap of 1.62 eV and in agreement with previous reports.^[29–32] The PL band of tetragonal perovskite is believed to originate from a near-band-edge transition.^[30–31,33] Up to 0.3 GPa, PL of the $I4/mcm$ structure shows a progressive red shift (1.62 to 1.61 eV). In this pressure regime, the DFT calculations find the band gap to decrease from 1.67 to 1.62 eV, in accord with the PL (Figure 4b).

With increasing PbI_6 octahedral tilt angles, the transition of the $Im\bar{3}$ polymorph to the suggested orthorhombic $Immm$ structure at 0.4 GPa leads to a blue-shifted PL spectra accompanying an increase of the band gap from 1.64 to 1.69 eV. The pressure-dependent PL variations are similar to those in the $MAPbBr_3$ system reported recently.^[26] The PL band weakens substantially beyond 2.0 GPa, and vanishes at 2.7 GPa with the destabilization of the $Im\bar{3}$ supercell. The PL spectra during decompression are also instructive. For example, when a peak-pressure of 6.4 GPa was applied, the PL was annihilated upon release of pressure. In contrast, from a peak-pressure of 3.5 GPa, weak PL band appears at 1.7 GPa, near the incipient recovery of the cubic supercell (Figures S4,S5).

As PL correlates directly with polymorphism, conversion from the low-pressure $I4/mcm$ phase into the cubic $Im\bar{3}$ supercell (< 0.4 GPa) offers a chemically independent means of reducing $MAPbI_3$ band gaps, or directing the design of novel organic–inorganic hybrid chemistries. When these two strategies are applied in tandem, the judicious selection of ionic ratios near polymorphic boundaries and the application

of relatively low pressures could be deployed to extend the absorption range over the long wavelength region for the future photovoltaic device design.

To better understand the atomistic origin of the PL in MAPbI₃, DFT calculations using the Perdew-Burke-Ernzerhof (PBE)^[34] approach were undertaken to optimize atomic positions, including London dispersion (van der Waals attraction) using the empirical D3 correction of Grimme et al.^[35] to account for the strong hydrogen bonding between MA cations and the tilted octahedra in MAPbI₃.^[36] The band gaps were then calculated using the B3PW91 flavor of DFT, which has been validated to yield band gaps accurate to approximately 0.09 eV.^[37] Spin-orbit coupling (SOC) makes a significant contribution in the MAPbI₃ system and was also included.^[38] Owing to the rotational disorder of MA, the high symmetry tetragonal and cubic phases were modelled using a 2 × 2 × 2 supercell, with two sets of MA cation configurations that are energetically close (Figure S8), and the band gap results were averaged according to Boltzmann distribution at room temperature (Table S4). The predicted pressure-dependent band gaps (Figure 4b), decreasing from 1.67 to 1.62 eV up to 0.3 GPa, while increasing from 1.58 to 1.74 eV between 0.4 to 2.0 GPa, are in excellent agreement with the experimental values (1.62 to 1.61 eV, 1.64 to 1.69 eV, respectively). The success of our prediction from averaging over configurations is consistent with the fact that both tetragonal and cubic phases are of thermally averaged structures.

In summary, the pressure-induced polymorphism and band-gap tuning of MAPbI₃ were investigated using synchrotron XRD, and the trends in band gap extracted from laser-excited photoluminescence (PL) spectra compared with the DFT calculations. As illustrated in Scheme 1, MAPbI₃ undergoes two high-pressure phase transformations from a tetragonal polymorph (*I4/mcm*) at ambient pressure, to a suggested

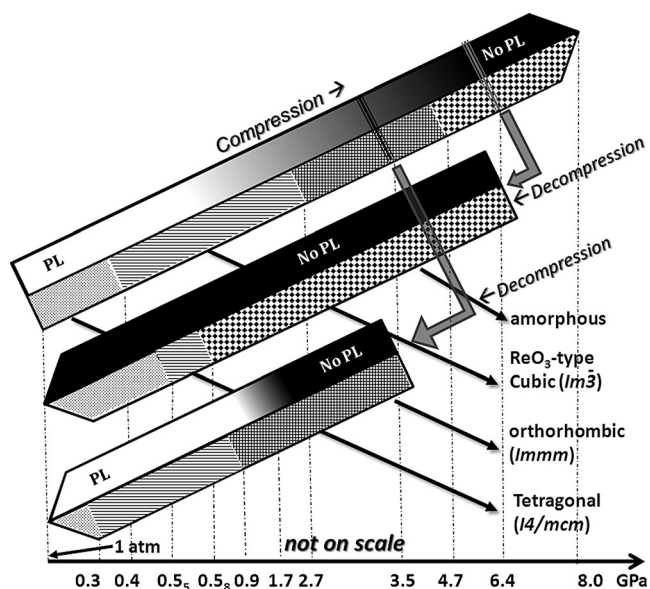
orthorhombic (*Immm*) form (2.7 GPa), through to an ReO₃-type (*Im* $\bar{3}$) cubic supercell (0.4–2.7 GPa), and finally amorphization above 2.7 GPa. The transition from *I4/mcm* to *Im* $\bar{3}$ leads to a smaller band gap energy, whereas conversion from the *Im* $\bar{3}$ polymorph into the suggested *Immm* polymorph reverses this trend. During decompression, crystallographic restoration was dependent on the peak-pressure achieved. Recovery from 6.4 GPa restored the *Im* $\bar{3}$ polymorph from the partially amorphized state at around 0.5 GPa. However, from a peak pressure of 3.5 GPa the same structure was recovered at 0.9 GPa owing to better preservation of long-range order at the 3.5 GPa compared to 6.4 GPa. These studies provide insights into the correlations between structure and band gap, uncompromised by changes in chemistry. Changes in power conversion efficiency (PCE) through the application of external pressure can be mimicked through chemical tailoring, where the introduction of ions in different sizes can effectively modify internal pressure and stabilize new polymorphs. By chemically adjusting hybrid perovskite compositions near to polymorphic boundaries, the application of modest pressure can be sufficient to initiate phase changes and band gap adjustments. This combined chemical–pressure strategy may prove valuable in the design of new perovskites for photovoltaic applications.

Acknowledgements

This work is partially supported by NRF-CRP14-2014-03, Custom Electronics, Inc., and the Joint Center for Artificial Photosynthesis, a DOE Energy Innovation Hub, supported through the Office of Science of the U.S. Department of Energy under Award No. DE-SC0004993. CHESS is supported by the NSF award DMR-1332208. S.J. acknowledges the support by Binghamton University.

Keywords: band gap · halide perovskite · high-pressure chemistry · phase transitions · photoluminescence

How to cite: *Angew. Chem. Int. Ed.* **2016**, *55*, 6540–6544
Angew. Chem. **2016**, *128*, 6650–6654



Scheme 1. A schematic illustration of structure transition of MAPbI₃ as a function of pressure (not on scale). “PL” represents photoluminescence observation. In the phases the top shading indicates with or without PL, the bottom shadings indicate different phases.

- [1] S. D. Stranks, G. E. Eperon, G. Grancini, C. Menelaou, M. J. Alcocer, T. Leijtens, L. M. Herz, A. Petrozza, H. J. Snaith, *Science* **2013**, *342*, 341–344.
- [2] G. Xing, N. Mathews, S. Sun, S. S. Lim, Y. M. Lam, M. Grätzel, S. Mhaisalkar, T. C. Sum, *Science* **2013**, *342*, 344–347.
- [3] N.-G. Park, *Mater. Today* **2015**, *18*, 65–72.
- [4] J. Burschka, N. Pellet, S.-J. Moon, R. Humphry-Baker, P. Gao, M. K. Nazeeruddin, M. Grätzel, *Nature* **2013**, *499*, 316–319.
- [5] H. Zhou, Q. Chen, G. Li, S. Luo, T.-b. Song, H.-S. Duan, Z. Hong, J. You, Y. Liu, Y. Yang, *Science* **2014**, *345*, 542–546.
- [6] N.-G. Park, *J. Phys. Chem. Lett.* **2013**, *4*, 2423–2429.
- [7] H. J. Snaith, *J. Phys. Chem. Lett.* **2013**, *4*, 3623–3630.
- [8] T.-B. Song, Q. Chen, H. Zhou, C. Jiang, H.-H. Wang, Y. M. Yang, Y. Liu, J. You, Y. Yang, *J. Mater. Chem. A* **2015**, *3*, 9032–9050.
- [9] Y. Zhao, K. Zhu, *J. Am. Chem. Soc.* **2014**, *136*, 12241–12244.
- [10] J. H. Noh, S. H. Im, J. H. Heo, T. N. Mandal, S. I. Seok, *Nano Lett.* **2013**, *13*, 1764–1769.

- [11] Z. Quan, Y. Wang, I.-T. Bae, W. S. Loc, C. Wang, Z. Wang, J. Fang, *Nano Lett.* **2011**, *11*, 5531–5536.
- [12] Y. Ma, M. Eremets, A. R. Oganov, Y. Xie, I. Trojan, S. Medvedev, A. O. Lyakhov, M. Valle, V. Prakapenka, *Nature* **2009**, *458*, 182–185.
- [13] T. Wang, R. Li, Z. Quan, W. S. Loc, W. A. Bassett, Y. C. Cao, J. Fang, Z. Wang, *Adv. Mater.* **2015**, *27*, 4544–4549.
- [14] A. M. Glazer, *Acta Crystallogr. Sect. B* **1972**, *28*, 3384–3392.
- [15] A. M. Glazer, *Acta Crystallogr. Sect. A* **1975**, *31*, 756–762.
- [16] B. Wang, X. Xiao, T. Chen, *Nanoscale* **2014**, *6*, 12287–12297.
- [17] F. Meillaud, A. Shah, C. Droz, E. Vallat-Sauvain, C. Miazza, *Sol. Energy Mater. Sol. Cells* **2006**, *90*, 2952–2959.
- [18] T. Ou, J. Yan, C. Xiao, W. Shen, C. Liu, X. Liu, Y. Han, Y. Ma, C. Gao, *Nanoscale* **2016**, *8*, <http://dx.doi.org/10.1039/C5NR07842C>.
- [19] T. Baikie, Y. Fang, J. M. Kadro, M. Schreyer, F. Wei, S. G. Mhaisalkar, M. Graetzel, T. J. White, *J. Mater. Chem. A* **2013**, *1*, 5628–5641.
- [20] H. K. Mao, J. Xu, P. M. Bell, *J. Geophys. Res.* **1986**, *91*, 4673–4676.
- [21] Z. Wang, O. Chen, C. Y. Cao, K. Finkelstein, D.-M. Smilgies, X. Lu, W. A. Bassett, *Rev. Sci. Instrum.* **2010**, *81*, 093902.
- [22] I. P. Swainson, M. G. Tucker, D. J. Wilson, B. Winkler, V. Milman, *Chem. Mater.* **2007**, *19*, 2401–2405.
- [23] E. Suzuki, Y. Kobayashi, S. Endo, T. Kikegawa, *J. Phys. Condens. Matter* **2002**, *14*, 10589–10593.
- [24] J.-E. Jorgensen, J. D. Jorgensen, B. Batlogg, J. P. Remeika, J. D. Axe, *Phys. Rev. B* **1986**, *33*, 4793–4798.
- [25] Y. Lee, D. B. Mitzi, P. W. Barnes, T. Vogt, *Phys. Rev. B* **2003**, *68*, 020103.
- [26] Y. Wang, X. Lü, W. Yang, T. Wen, L. Yang, X. Ren, L. Wang, Z. Lin, Y. Zhao, *J. Am. Chem. Soc.* **2015**, *137*, 11144–11149.
- [27] T. Baikie, N. S. Barrow, Y. Fang, P. J. Keenan, P. R. Slater, R. O. Piltz, M. Gutmann, S. G. Mhaisalkar, T. J. White, *J. Mater. Chem. A* **2015**, *3*, 9298–9307.
- [28] C. C. Stoumpos, C. D. Malliakas, M. G. Kanatzidis, *Inorg. Chem.* **2013**, *52*, 9019–9038.
- [29] S. Colella, E. Mosconi, P. Fedeli, A. Listorti, F. Gazza, F. Orlandi, P. Ferro, T. Besagni, A. Rizzo, G. Calestani, *Chem. Mater.* **2013**, *25*, 4613–4618.
- [30] Y. Yamada, T. Nakamura, M. Endo, A. Wakamiya, Y. Kanemitsu, *Appl. Phys. Express* **2014**, *7*, 032302.
- [31] W. Kong, Z. Ye, Z. Qi, B. Zhang, M. Wang, A. Rahimi-Iman, H. Wu, *Phys. Chem. Chem. Phys.* **2015**, *17*, 16405–16411.
- [32] J. Qiu, Y. Qiu, K. Yan, M. Zhong, C. Mu, H. Yan, S. Yang, *Nanoscale* **2013**, *5*, 3245–3248.
- [33] C. Wehrenfennig, M. Liu, H. J. Snaith, M. B. Johnston, L. M. Herz, *J. Phys. Chem. Lett.* **2014**, *5*, 1300–1306.
- [34] J. P. Perdew, K. Burke, M. Ernzerhof, *Phys. Rev. Lett.* **1996**, *77*, 3865–3868.
- [35] S. Grimme, J. Antony, S. Ehrlich, H. Krieg, *J. Chem. Phys.* **2010**, *132*, 154104.
- [36] J.-H. Lee, N. C. Bristowe, P. D. Bristowe, A. K. Cheetham, *Chem. Commun.* **2015**, *51*, 6434–6437.
- [37] H. Xiao, J. Tahir-Kheli, W. A. Goddard III, *J. Phys. Chem. Lett.* **2011**, *2*, 212–217.
- [38] P. Umari, E. Mosconi, F. D. Angelis, *Sci. Rep.* **2014**, *4*, 4467.

Received: February 19, 2016

Published online: April 21, 2016